



RESEARCH ARTICLE | SEPTEMBER 07 2018

Stretchable IR metamaterial with ultra-narrowband perfect absorption

Ruijia Xu; Ji Luo; Jun Sha; Jitong Zhong; Zefeng Xu; Yanlin Tong; Yu-Sheng Lin  



Appl. Phys. Lett. 113, 101907 (2018)

<https://doi.org/10.1063/1.5044225>



Articles You May Be Interested In

Large-sized out-of-plane stretchable electrodes based on poly-dimethylsiloxane substrate

Appl. Phys. Lett. (December 2014)

Kirigami stretchable strain sensors with enhanced piezoelectricity induced by topological electrodes

Appl. Phys. Lett. (June 2018)

A stretchable and screen-printable conductive ink for stretchable electronics

Appl. Phys. Lett. (November 2016)

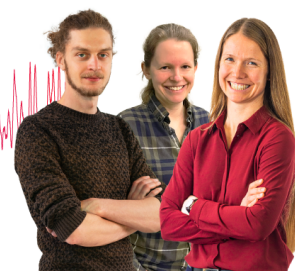
Webinar From Noise to Knowledge

May 13th – Register now



Zurich
Instruments

Universität
Konstanz



Stretchable IR metamaterial with ultra-narrowband perfect absorption

Ruijia Xu, Ji Luo, Jun Sha, Jitong Zhong, Zefeng Xu, Yanlin Tong, and Yu-Sheng Lin^{a)}

State Key Laboratory of Optoelectronic Materials and Technologies, School of Electronics and Information Technology, Sun Yat-Sen University, Guangzhou 510275, China

(Received 12 June 2018; accepted 24 August 2018; published online 7 September 2018)

The integration of a high-performance metamaterial (MM) onto mechanically flexible and deformable substrates offers significant promise in flexible electronics. Here, we propose two types of stretchable infrared (IR) MMs to design a tunable perfect absorber with a ring-shape (PA-RS) and a cross-shape (PA-CS) on a PDMS/Au/PDMS substrate, respectively. By stretching devices along different directions, PA-RS and PA-CS exhibit ultra-narrowband, polarization-dependent/independent, and switchable characterizations in the IR wavelength range. The tuning ranges are $2.37\ \mu\text{m}$ and $2.36\ \mu\text{m}$ for PA-RS and PA-CS with the deformation quantity of $2.50\ \mu\text{m}$ along two-dimensional directions, respectively, without extra power supply. In this deformation range, most of the incident light is perfectly absorbed for PA-RS design operated at a wavelength of $4.31\ \mu\text{m}$ and PA-CS design operated at a wavelength of $4.24\ \mu\text{m}$. The corresponding Q-factors of two devices are 98 and 118 for PA-RS and PA-CS, respectively. Such results are very suitable for high-performance refractive index sensor applications. Furthermore, two devices exhibit the functionalities of s-polarization switches and s/p-polarization switches. To further investigate the characterizations of devices deformed by a tensile force, PA-CS could be actively tuned by bending devices at a certain angle. In the future, these proposed stretchable IR MMs could potentially possess high portability, applicability, and cost-effectiveness for wearable electronic devices in a variety of sensor fields. *Published by AIP Publishing.* <https://doi.org/10.1063/1.5044225>

Metamaterials (MMs) are artificial materials that can manipulate electromagnetic (EM) waves on subwavelength scales to exhibit unique EM responses and enhance optical performance by proper tailoring. The EM response of MMs can be designed through the manipulation of the pattern, size, and composition of their subwavelength unit cells. They are widely studied in cloaking devices, high-sensitive sensors, perfect absorbers (PAs), security screening, medical imaging, and non-destructive testing due to the extraordinary properties that cannot be found in nature.^{1–3} Recently, MMs have been proposed to achieve nearly 100% absorption in the wide wavelength range of the EM spectrum, starting from microwaves to near infrared (IR) and visible light.⁴ For a narrowband perfect absorber, the desire to realize a high quality factor (Q-factor) and strong absorption intensity has long been a research topic of interest for scientists. Among these designs of the narrowband absorber, they have been demonstrated by using graphene materials,⁵ all-metallic structures,⁶ metal-dielectric-metal structures,^{7,8} and so on. To increase the flexibility of MM, there are literatures reporting the tuning mechanisms, including semiconductor diodes,⁹ ferroelectric materials,¹⁰ thermal annealing,¹¹ laser pumping,¹² and liquid crystals.¹³ In these tuning approaches, reconfigurable MMs become feasible in many applications, such as sensors, switches, and filters other than the use of liquid crystals, ferroelectric materials, and semiconductor diodes which are highly dependent on the nonlinear properties of the nature material. These methods suffer from a limited tuning range.

To improve the tuning range and performance of EM characteristics, we present a different approach and exploit

the elasticity of a compliant substrate to tune the resonant wavelength of MM by reconfiguring the period of the device. The uses of flexible and elastomeric substrates to modify the optical properties of MM have been reported,^{14–16} including the uses of polydimethylsiloxane (PDMS), polyimide, polyethylene terephthalate (PET), polyethylene naphthalene (PEN), Kapton, and so on. Among these polymer substrate materials, PDMS has been commonly used as a flexible substrate due to the properties of low electrical losses and excellent mechanical performance. Therefore, we propose that the integration of functional high-performance IR absorbers onto mechanically flexible and deformable PDMS substrates offers significant promise in flexible electronics, e.g., flexible displays,¹⁷ solar cells,¹⁸ refractive index sensors,¹⁹ thermal emitters,^{20,21} and optical filters.²² Compared to rigid and flat substrates, e.g., silicon and quartz, flexible and stretchable PDMS-based substrates exhibit great advantages of flexibility, transparency, lightweight, portability, low cost, conformable manipulation, and biocompatibility.

In this study, we propose an active tuning approach to control IR MMs for ultra-narrowband perfect absorber (PA) applications by using Lumerical Solution's finite difference time domain (FDTD) based simulations to study the optical properties of the designed MMs. The propagation direction of incident light is set to be perpendicular to the x - y plane in the numerical simulations. Periodic boundary conditions are also adopted in the x and y directions, and perfectly matched layer (PML) boundaries conditions are assumed in the z direction. The reflection (R) and transmission (T) of lights are calculated by two monitors set on both sides of the device. This method is without extra power supply, i.e., using the mechanical deformation of elastomeric substrates to perform stretchable IR MMs. We demonstrate tunable IR

^{a)} Author to whom correspondence should be addressed: linyoush@mail.sysu.edu.cn

MMs with different optical characteristics by changing directions of stretchable force applied on devices, i.e., stretching along one-dimensional and two-dimensional directions. It shows that the tuning range is $2.36 \mu\text{m}$ with the deformation quantity of $2.50 \mu\text{m}$ for two-dimensional directions. In this deformation range, most of the incident light is perfectly absorbed at a $4.24 \mu\text{m}$ wavelength, and the corresponding Q-factor is 118 higher than those reported in literatures.²⁰⁻²³ These proposed PA devices exhibit the functionalities of s-polarization switches and s/p-polarization switches. Furthermore, PA devices could be actively tuned by bending devices at a certain angle, which shows great tunability of EM responses. It is very suitable for wearable electronic device applications. By changing the surrounding refractive index, absorption resonance of PA shifts to a longer wavelength, which can be used as a high-performance refractive index sensor.

Figures 1(a) and 1(b) show the proposed PA with ring shape (PA-RS) and cross-shape (PA-CS) structures, respectively, on the PDMS elastic substrate. The structural compositions are Au/PDMS/Au/PDMS from top to bottom. The top Au thin-film with a thickness of 200 nm was tailored to form ring and cross shapes on the PDMS/Au/PDMS substrate. It is regarding the direction of stretchable force applied on devices, resulting in different geometric deformations. Two methods to stretch PA-RS and PA-CS are represented. They are stretching along the x -axis and xy -axes as shown in inserted schematic coordinates of Fig. 1, where E , H , and k are the electric field, magnetic field, and wavevector of the incident EM wave, respectively. The p-polarization (transverse electric mode) and s-polarization (transverse magnetic mode) are defined as the incident light normally propagated through the device along the z -direction, while the electric field (E) and the magnetic field (H) are along the x -direction, respectively. Here, for the one-dimensional case, i.e., stretching along the x -axis, the deformation can be expressed as

$$\varepsilon_x = \sigma_x / E, \quad (1)$$

where ε_x is the ratio of the length change to initial length, σ_x is the strain of PDMS along the x -axis, and E is the Young's modulus of PDMS. In another situation, by stretching along

two directions, i.e., stretching along xy -axes, the deformation can be expressed as

$$\varepsilon_{xy} = \sigma_{xy} / E, \quad (2)$$

where ε_{xy} is the ratio of the whole area change to initial area and σ_{xy} is the strain of PDMS along xy -axes.

Herein, the absorption (A) is defined as $1-R-T$, where R and T are the reflection and transmission. Since transmission is inhibited by the opaque embedded Au layer, then A can be directly obtained by $A=1-R$. Therefore, the target is to design PA-RS and PA-CS with zero reflection. According to the theory of the Drude-Lorentz model,²⁴ the resonant wavelength of the proposed device is a function of the effective refractive index of EM radiation, i.e., $n_{\text{eff}} = \sqrt{\varepsilon_{\text{eff}} \mu_{\text{eff}}}$, where ε_{eff} and μ_{eff} are the effective permittivity and permeability of MM and the incident medium is lossless at normal incidence. The optical response can be calculated by optical impedance (Z) of an interface as expressed by the following equation:²⁵

$$Z = \pm \sqrt{\frac{(1+r)^2 - t^2}{(1-r)^2 - t^2}}, \quad (3)$$

where r and t are the reflection coefficient and transmission coefficient, respectively. The real and imaginary refractive index (n_{eff}) must be determined using the following equations:²⁶

$$\text{Im}(n_{\text{eff}}) = \pm \text{Im} \left\{ \frac{\cos^{-1} \left[\frac{1}{2t} (1 - r^2 + t^2) \right]}{kd} \right\}, \quad (4)$$

$$\text{Re}(n_{\text{eff}}) = \pm \text{Re} \left\{ \frac{\cos^{-1} \left[\frac{1}{2t} (1 - r^2 + t^2) \right]}{kd} \right\} + \frac{2m\pi}{kd}, \quad (5)$$

where d is the MM thickness, k is the incident wavevector, and m is an integer used to correct branch errors.²⁶ μ_{eff} and ε_{eff} can be found as $\mu_{\text{eff}} = n_{\text{eff}} Z$ and $\varepsilon_{\text{eff}} = n_{\text{eff}} / Z$ and then expressed by $Z = \sqrt{\mu_{\text{eff}} / \varepsilon_{\text{eff}}} = 1$. Therefore, the unit cell of PA-RS and PA-CS can achieve zero reflection. Owing to this, it can have an impedance equal to the free space value which is indicated as $Z = 1$. The impedance matching of PA-RS and PA-CS results from EM optical resonance, which is induced by the dipole/image interaction and causes an EM confinement between the MMs and thereby eliminates the reflection. The approximated capacitance (C) between neighboring resonators is expressed by the following equation:

$$C = \frac{\varphi \varepsilon_0 \varepsilon_d W d}{P - L}, \quad (6)$$

where φ is the numerical factor to approximate the non-uniform distribution of charges due to the induced electric currents, ε_0 is the permittivity in free space, ε_d is the relative permittivity, and W , L , d , and P are the width, length, thickness, and period of the MM unit cell, respectively. Therefore, the active tunabilities of PA-RS and PA-CS could be achieved without extra power supply by increasing P and then decreasing C . Figures 1(c) and 1(d) show two types of

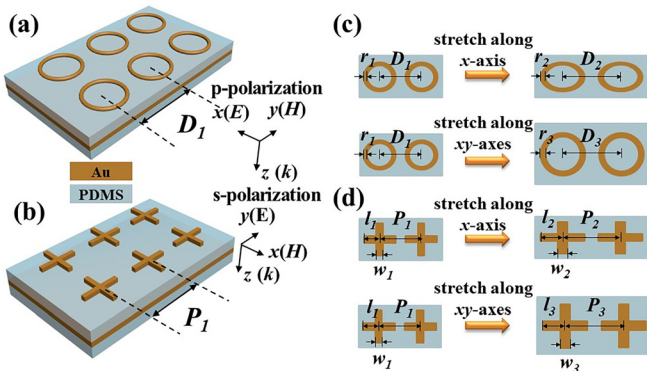


FIG. 1. Three-dimensional schematic drawings of (a) PA-RS and (b) PA-CS, where E , H , and k are the electric field, magnetic field, and wavevector of the incident EM wave, respectively. (c) and (d) are illustrations of stretched PA-RS and PA-CS, respectively. Geometrical dimensions are $D_1 = P_1 = 3 \mu\text{m}$, $r_1 = 0.072 \mu\text{m}$, $l_1 = 1.2 \mu\text{m}$, and $w_1 = 0.3 \mu\text{m}$.

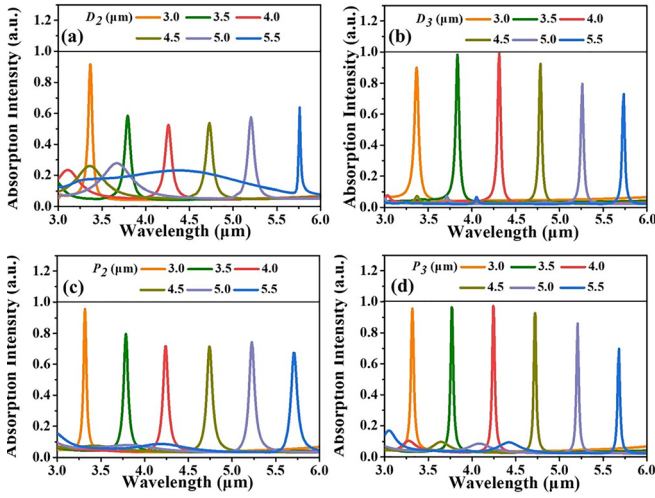


FIG. 2. Absorption intensities of PA-RS stretched along (a) x -axis and (b) xy -axes directions and PA-CS stretched along (c) x -axis and (d) xy -axes directions, respectively.

stretch directions of PA-RS and PA-CS, respectively. The stretch force applied on devices along the x -axis and xy -axes will deform the structural geometries. For the deformation of PA-RS and PA-CS, the changes of structural widths (r_l , l_l , w_l) are proportional to periods (D_l , P_l), which means the structural deformation related to the period parameter directly.

Figure 2 shows the absorption spectra of the stretched PA-RS and PA-CS operated at p-polarization in the IR wavelength range. Four parameters (D_2 , D_3 , P_2 , and P_3) are modified to describe the deformation of four different shapes. Figure 2(a) indicates that the absorption resonance shifts to a longer wavelength by stretching PA-RS along the x -axis, i.e., increasing the period of PA-RS (D_2). The tuning range of absorption resonance is $2.37 \mu\text{m}$ from $D_2 = 3.0 \mu\text{m}$ to $D_2 = 5.5 \mu\text{m}$. When PA-RS is stretched along xy -axes, the absorption intensity is increased and then decreased from $D_3 = 3.0 \mu\text{m}$ to $D_3 = 5.5 \mu\text{m}$. The tuning range is $2.37 \mu\text{m}$ as shown in Fig. 2(b). It is clearly observed that most of the incident light is perfectly absorbed in PA-RS at the stretch condition of $D_3 = 4 \mu\text{m}$ at the $4.3 \mu\text{m}$ wavelength. There are identical EM responses for PA-CS design as shown in Figs. 2(c) and 2(d). The stretch force applied on devices along xy -axes exhibits higher absorption intensity than that along the x -axis. The performance of proposed PA-RS and PA-CS is

characterized by their Q-factors expressed as $Q = \lambda/\text{FWHM}$, where λ is the resonant wavelength and FWHM is the full width at half maximum of the resonant wavelength. The Q-factors are 98 and 44 for PA-RS stretched along xy -axes and the x -axis at $4.31 \mu\text{m}$ and $4.26 \mu\text{m}$ wavelengths, respectively. For PA-CS stretched along xy -axes and the x -axis, Q-factors are 118 and 54 at $4.24 \mu\text{m}$ and $4.23 \mu\text{m}$ wavelengths, respectively. The Q-factor is enhanced 2.2-fold to perform the ultra-narrowband characterization. It can be concluded that the IR MMs stretched along xy -axes possess obviously higher performance in absorption characteristic than those stretched along the x -axis. Figure 3 shows side views of simulated E-field and H-field distributions of PA-RS and PA-CS with periods of $4 \mu\text{m}$. It indicates the higher H-field intensity between the top MM layer and the bottom metal layer. Such designs form an optical cavity where the light is confined and gradually absorbed by the metallic layers. Compared with PA-RS stretched along the x -axis, the EM resonance in PA-RS stretched along xy -axes absorbed more EM spectrum in the top MM layer. It shows identical absorption characteristic for PA-CS stretched along the x -axis and xy -axes, respectively.

The collection of absorption resonances operated at s-polarization and p-polarization is indicated as shown in Fig. 4. In Fig. 4(a), the absorption intensities are almost zero for two devices stretched along the x -axis operated at s-polarization. For two devices stretched along xy -axes operated at s-polarization, the absorption intensities are over 0.7 even reaching the ideal perfect absorption. The optical behaviors of stretch force applied along xy -axes are identical for s-polarization [Fig. 4(a)] and p-polarization [Fig. 4(b)]. It means that these two devices are polarization-independent operated at two stretch directions, i.e., along xy -axes. Furthermore, the optical behaviors of stretch force applied along the x -axis are different for s-polarization [Fig. 4(a)] and p-polarization [Fig. 4(b)]. It can be seen that two devices are polarization-dependent operated at one stretch direction, i.e., along the x -axis. The comparison of devices operated along the x -axis and xy -axes at s-polarization is shown in Fig. 4(a). Two devices exhibit the switching function of the s-wave. They could be tuned by one or two directions to turn on s-wave or turn off it. Such designs of proposed stretchable IR MMs may serve as a highly efficient IR filter, IR polarizer and IR switch and could potentially be used in various sensors.

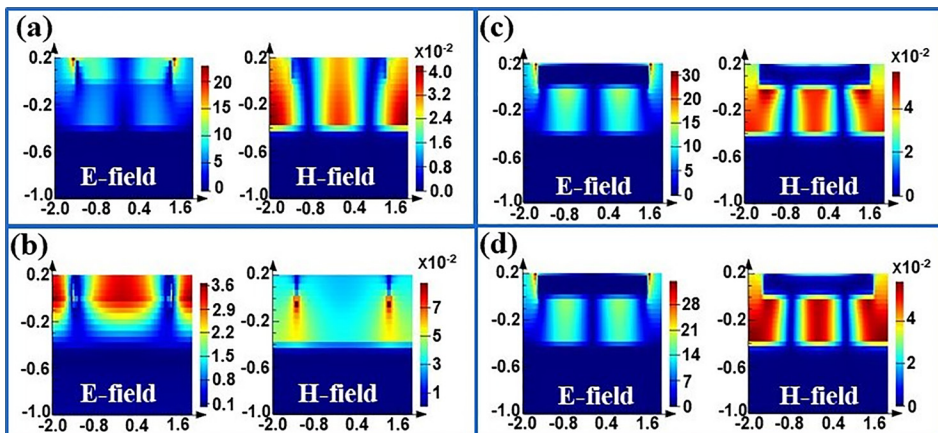


FIG. 3. Side views of E-field and H-field distributions of PA-RS stretched along (a) x -axis and (b) xy -axes directions and PA-CS stretched along (c) x -axis and (d) xy -axes directions, respectively, while the corresponding monitors are at $4.26 \mu\text{m}$, $4.31 \mu\text{m}$, $4.23 \mu\text{m}$, and $4.24 \mu\text{m}$ wavelengths for (a), (b), (c), and (d), respectively. D_2 , D_3 , P_2 , and P_3 are kept at $4 \mu\text{m}$.

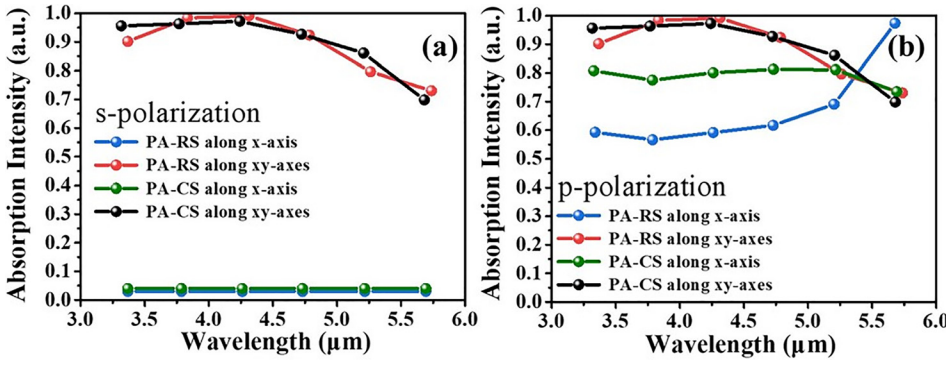


FIG. 4. Absorption intensities of PA-RS and PA-CS stretched along the x -axis and xy -axes at (a) s-polarization and (b) p-polarization, respectively.

To further investigate that the two devices can be potentially used as environmental sensors, the relationship of absorption resonances of devices and the surrounding refractive index is studied as shown in Fig. 5. PA-RS and PA-CS with periods of $4\ \mu\text{m}$ stretched along xy -axes are chosen for refractive index sensing applications as shown in Fig. 5(a) for PA-RS and Fig. 5(b) for PA-CS. The absorption resonance is red-shifted by increasing the refractive index from 1.0 to 1.4. The absorption intensity decreases gradually from 1.0 to 1.2 and sharply from 1.2 to 1.4. There is almost no absorption with the refractive index more than 1.4 for both the devices. The corresponding linear relationship of the absorption resonance and surrounding refractive index is clearly observed as shown in Figs. 5(c) and 5(d) for PA-RS and PA-CS, respectively. It is worth noting that the correlation coefficient is 0.9999 for two devices, which is very suitable for refractive index sensing applications and can enhance the sensitivity of the refractive index sensor owing to the ultra-narrowband of IR absorption resonance.

For wearable electronic device applications, PA-CS with different bending angles is illustrated in Fig. 6. The inset image is three-dimensional schematic drawing of PA-CS stretched along the z -axis direction and the corresponding top views of E-field and H-field distributions of PA-CS,

respectively. By increasing the bending angle, the absorption resonance is red-shifted and the bandwidth becomes broad, while the absorption intensity is gradually lower as shown in Fig. 6. The absorption intensity of PA-CS with the bending angle of 0° is 95% at the $3.31\ \mu\text{m}$ wavelength, which will decay to 21% at the $3.58\ \mu\text{m}$ wavelength with a bending angle of 50° . The corresponding Q-factor also decreases greatly. In view of this, characterization of PA-CS was performed, which exhibits a switching function by bending PA-CS with a certain angle. In the top views of E-field and H-field distributions of PA-CS with bending angles of 0° , 20° , and 50° , the EM spectrum at absorption resonance becomes weaker by increasing the bending angle. Such flexible IR MMs exhibit active tunability and could serve as wearable electronic devices.

In conclusion, two types of stretchable IR MMs are proposed to realize an ultra-narrowband perfect absorber. The tuning IR wavelength ranges are $2.37\ \mu\text{m}$ and $2.36\ \mu\text{m}$ for PA-RS and PA-CS with the deformation quantity of $2.50\ \mu\text{m}$ along xy -axes, respectively. For PA-RS operated at the $4.31\ \mu\text{m}$ wavelength and PA-CS operated at the $4.24\ \mu\text{m}$ wavelength, most of the light can be absorbed thoroughly. The corresponding Q-factors are 98 and 118 for PA-RS and PA-CS, respectively. They exhibit ultra-narrowband IR absorption stretched along xy -axes to have high absorption intensities and high Q-factors. Furthermore, two devices are

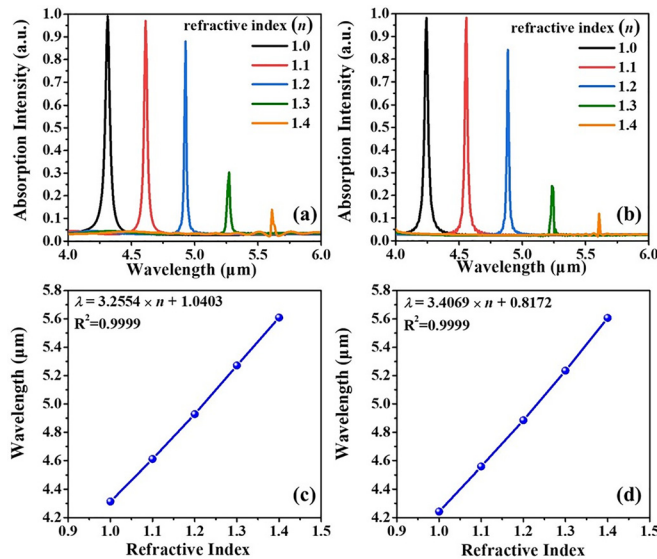


FIG. 5. Absorption intensities of (a) PA-RS and (b) PA-CS stretched along xy -axes with different surrounding refractive indices. The corresponding relationship of the resonance and refractive index for (c) PA-RS and (d) PA-CS. D_3 and P_3 are kept at $4\ \mu\text{m}$.

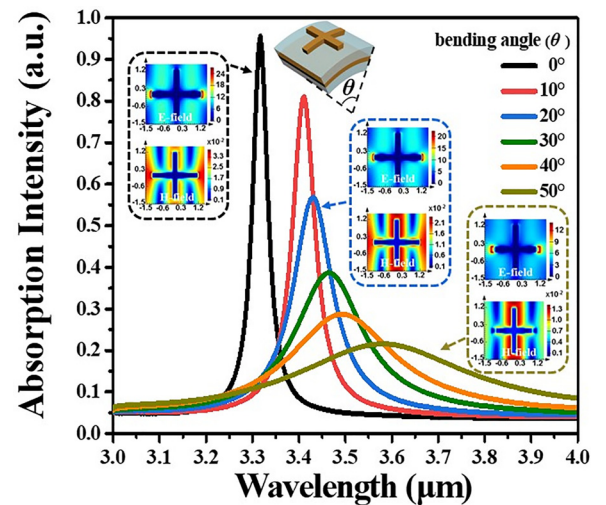


FIG. 6. Absorption intensities of PA-CS stretched along the z -axis in different bending angles from 0° to 50° . The inset image is the 3D schematic drawing of PA-CS stretched along the z -axis direction and the corresponding top views of E-field and H-field distributions of PA-CS, respectively. P_1 is kept at $3\ \mu\text{m}$.

not only polarization-dependent by stretch force along the x -axis but also polarization-independent by stretch force along xy -axes, which could serve as s-polarization switches and s-/p-polarization switches. The absorption resonances of devices shift to a longer wavelength by changing the surrounding refractive index. The corresponding relationship of the absorption resonance and refractive index is linear with a correlation coefficient of 0.9999. For wearable electronic device applications, PA-CS exhibits active tunability by the bending device with a certain angle. By increasing the bending angle, the absorption resonance is red-shifted and absorption intensity is lower. Using stretch force modifies the geometric shape of the proposed devices, which could be used as filters, polarizers, switches, and absorbers to have multi-functionalities. Such designs provide that the stretchable IR MMs can be realized in wearable electronic devices without extra power supply and can be used for widespread applications in the future, e.g., IR sensors, strain gauges, pressure sensors, and so on.

¹Y. S. Lin, F. Ma, and C. Lee, *Opt. Lett.* **38**, 3126–3128 (2013).

²Y. S. Lin, C. Y. Huang, and C. Lee, *IEEE J. Sel. Top. Quantum Electron.* **21**(4), 2700207 (2015).

³D. Hasan and C. Lee, *Adv. Sci.* **5**, 1700581 (2018).

⁴D. Wu, R. Li, Y. Liu, Z. Yu, L. Yu, L. Chen, C. Liu, R. Ma, and H. Ye, *Nanoscale Res. Lett.* **12**, 427 (2017).

⁵L. P. Sun, X. Zhai, Q. Lin, G. D. Liu, and L. L. Wang, *Plasmonics* **13**, 1043–1048 (2018).

⁶Z. Li, S. Butun, and K. Aydin, *ACS Nano* **8**, 8242–8248 (2014).

⁷D. Wu, Y. Liu, R. Li, L. Chen, R. Ma, C. Liu, and H. Ye, *Nanoscale Res. Lett.* **11**, 483 (2016).

⁸S. Li, X. Ai, R. Wu, and J. Chen, *Opt. Mater.* **73**, 111–118 (2017).

⁹Y. C. Jun and I. Brener, *J. Opt.* **14**, 114013 (2012).

¹⁰Y. Zhang, X. Hu, Y. Fu, H. Yang, and Q. Gong, *Appl. Phys. Lett.* **100**, 031106 (2012).

¹¹J. Y. Ou, E. Plum, L. Jiang, and N. I. Zheludev, *Nano Lett.* **11**, 2142–2144 (2011).

¹²H. Ji, B. Zhang, G. Wang, W. Wang, and J. Shen, *Opt. Commun.* **412**, 37–40 (2018).

¹³O. Buchnev, J. Y. Ou, M. Kaczmarek, N. I. Zheludev, and V. A. Fedotov, *Opt. Express* **21**, 1633–1638 (2013).

¹⁴S. Walia, C. M. Shah, P. Gutruf, H. Nili, D. R. Chowdhury, W. Withayachumnankul, M. Bhaskaran, and S. Sriram, *Appl. Phys. Rev.* **2**, 011303 (2015).

¹⁵I. M. Pryce, K. Aydin, Y. A. Kelaita, R. M. Briggs, and H. A. Atwater, *Nano Lett.* **10**, 4222 (2010).

¹⁶M. Apanius, P. B. Kaul, and A. R. Abramson, *Sens. Actuators, A* **140**, 168 (2007).

¹⁷M. C. Choi, Y. Kim, and C. S. Ha, *Prog. Polym. Sci.* **33**, 581–630 (2008).

¹⁸J. You, Z. Hong, Y. M. Yang, Q. Chen, M. Cai, T. Song, C. Chen, S. Lu, Y. Liu, H. Zhou, and Y. Yang, *ACS Nano* **8**, 1674–1680 (2014).

¹⁹Y. Chuo, D. Hohertz, C. Landrock, B. Omrane, K. L. Kavanagh, and B. Kaminska, *IEEE Sens. J.* **13**, 3982 (2013).

²⁰A. Lochbaum, Y. Fedoryshyn, A. Dorodnyy, U. Koch, C. Hafner, and J. Leuthold, *ACS Photonics* **4**, 1371–1380 (2017).

²¹H. T. Miyazaki, T. Kasaya, H. Oosato, Y. Sugimoto, B. Choi, M. Iwanaga, and K. Sakoda, *Sci. Technol. Adv. Mater.* **16**, 035005 (2015).

²²Y. L. Ho, M. Abasaki, S. Yin, X. Liu, and J. J. Delaunay, *Nanotechnology* **27**, 425202 (2016).

²³Y. Cheng, X. S. Mao, C. Wu, L. Wu, and R. Z. Gong, *Opt. Mater.* **53**, 195–200 (2016).

²⁴C. M. Soukoulis, M. Kafesaki, and E. N. Economou, *Adv. Mater.* **18**, 1941–1952 (2006).

²⁵X. Chen, T. M. Grzegorzczak, B.-I. Wu, J. Pacheco, Jr., and J. A. Kong, *Phys. Rev. E* **70**, 016608 (2004).

²⁶D. R. Smith, S. Schultz, P. Markos, and C. M. Soukoulis, *Phys. Rev. B* **65**, 195104 (2002).